Graphene: Corrosion-Inhibiting Coating

Dhiraj Prasai,[†] Juan Carlos Tuberquia,[§] Robert R. Harl,[§] G. Kane Jennings,[§] and Kirill I. Bolotin[‡,*]

[†]Interdisciplinary Graduate Program in Materials Science, [‡]Department of Physics and Astronomy, [§]Department of Chemical and Biomolecular Engineering, Vanderbilt University, Nashville, Tennessee 37235, United States

ABSTRACT

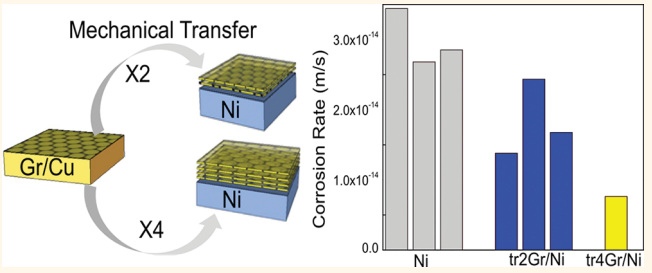

We report the use of atomically thin layers of graphene as a protective coating that inhibits corrosion of underlying metals. Here, we employ electrochemical methods to study the corrosion inhibition of copper and nickel by either growing graphene on these metals, or by mechanically transferring multilayer graphene onto them. Cyclic voltammetry measurements reveal that the graphene coating effectively suppresses metal oxidation and oxygen reduction. Electrochemical impedance spectroscopy measurements suggest that while graphene itself is not damaged, the metal under it is corroded at cracks in the graphene film. Finally, we use Tafel analysis to quantify the corrosion rates of samples with and without graphene coatings. These results indicate that copper films coated with graphene grown *via* chemical vapor deposition are corroded 7 times slower in an aerated Na_2SO_4 solution as compared to the corrosion rate of bare copper. Tafel analysis reveals that nickel with a multilayer graphene film grown on it corrodes 20 times slower while nickel surfaces coated with four layers of mechanically transferred graphene corrode 4 times slower than bare nickel. These findings establish graphene as the thinnest known corrosion-protecting coating.

KEYWORDS: graphene · copper · nickel · corrosion · Tafel · EIS

An intense effort is underway to find coatings that inhibit the process of metal corrosion, a problem costing US industries more than $200 billion annually.[1] Corrosion can be inhibited or controlled by introducing a stable protective layer made of inert metals,[2] conductive polymers,[3] or even thiol-based monolayers[4] between a metal and a corrosive environment. However, these protective coatings have their limitations. Thiolated SAMs can only be assembled onto some metals (*e.g.*, gold and copper) and do not withstand temperatures higher than ~100 °C.[5] Polymeric coatings are relatively thick and may significantly change the physical properties of the underlying material. Recent advances in the growth techniques of graphene[8] are expected to enable commercial viability of large-area graphene films.

Graphene, a single atomic monolayer of graphite, possesses a unique combination of properties that are ideal for corrosion-inhibiting coating in applications such as microelectronic components (*e.g.*, interconnects, aircraft components, and implantable devices). Graphene is chemically inert, stable in ambient atmosphere up to 400 °C,[6] and can be grown on the meter-scale and mechanically transferred onto arbitrary surfaces.[7] Both single-layer and multilayer graphene films are exceptionally transparent (>90% transmittance for 4-layered graphene[8,9]), so graphene coatings do not perturb the optical properties of the underlying metal. Recently, several pioneering experiments have demonstrated that graphene can effectively decouple the surface under it from the environment. First, Bunch *et al.* have shown that single-atomic graphene films are impermeable to gas molecules.[10] Second, Chen *et al.* have demonstrated that graphene can inhibit the oxidation of the underlying copper metal.[11]

Here, we take the next step and investigate the potential use of graphene as a corrosion protective coating, quantify the degree of corrosion inhibition, and explore the ways to enhance this behavior. We demonstrate that a coating of graphene inhibits the rate of corrosion of metals such as copper, on which graphene is grown by chemical vapor deposition (CVD) or of other materials, onto which large-scale graphene can be mechanically transferred. We explore the ways to increase the degree of protection by transferring multiple graphene layers onto target surfaces, thereby building thicker and more robust films. Finally, we show that electrochemical

* Address correspondence to kirill.bolotin@vanderbilt.edu.

Received for review September 12, 2011 and accepted February 2, 2012.

Published online February 02, 2012
10.1021/nn203507y

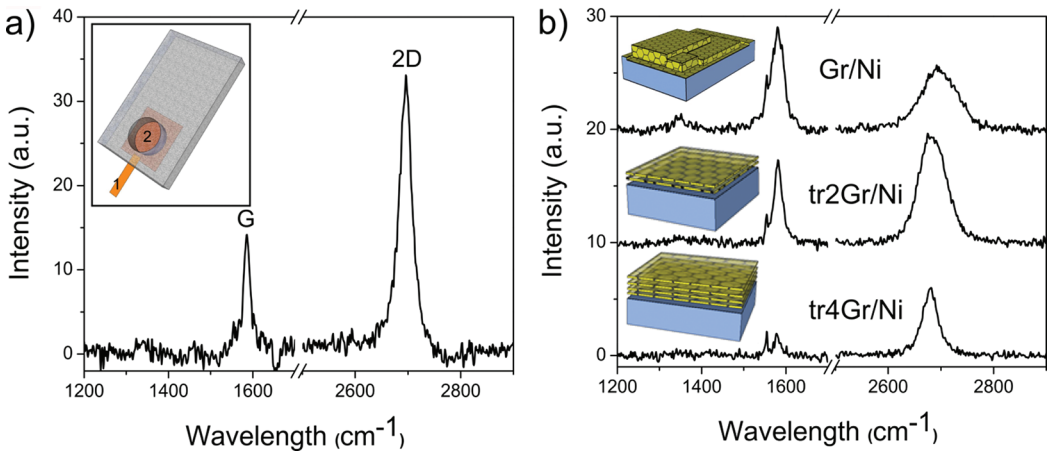

Figure 1. (a) Gr/Cu sample prepared via chemical vapor deposition, and its Raman spectrum exhibiting characteristic G and 2D peaks. Inset represents schematic of foils mounted onto PTFE 3-electrode cell where copper tape (1) is attached to the sample and 0.4 cm^2 of active area (2) is exposed to the $NaSO_4$ electrolyte. (b) Gr/Ni sample (patches of multilayer graphene grown *via* chemical vapor deposition on Ni) and tr2Gr/Ni and tr4Gr/Ni samples, where graphene was mechanically transferred onto nickel surface, along with their respective Raman spectra.

techniques such as Tafel analysis can help us measure the corrosion rates and that electrochemical impedance spectroscopy can be used to elucidate the pathways of corrosion reactions and quantify the presence of defects in graphene coatings. We expect that the described techniques for creating atomically thin graphene coatings and the approaches for their noninvasive characterization may significantly advance the field of corrosion protection.

RESULTS AND DISCUSSION

Sample Preparation. We investigated the corrosion-protection properties of graphene coatings on two prototypical metals, nickel and copper. These metals were chosen as they are technologically relevant, readily corrode in aqueous environments, and graphene films can either be grown or mechanical transferred onto them. We fabricated seven different kinds of samples to study the effect of graphene coatings on corrosion. First, to obtain baseline corrosion rates, we obtained bare copper samples (labeled "Cu") and bare nickel samples, (labeled "Ni"). Cu samples are copper foils (Alfa Aesar item no. 13382) that were annealed at 1000 °C for 1 h in the presence of 2 sccm of H_2 to remove surface contamination. Ni samples were prepared from 100 nm of thermally evaporated nickel on top of SiO_2/Si wafers with 4 nm of chrome adhesion layer. Second, we obtained samples with graphene grown on either copper ("Gr/Cu", produced on-site) or nickel ("Gr/Ni", Graphene Supermarket, Item No. SKU-CVD-04) *via* CVD. We grow Gr/Cu using the well-established recipes that yield high-quality, predominantly single layer graphene in the case of Gr/Cu,[7] as confirmed by Raman spectroscopy (Figure 1a). Cu foils, 25 μm thick, are cut into small strips and placed inside a fused silica tube and heated using a hot wall furnace. The Cu foil is first heated at 1000 °C under a 2 sccm flow of hydrogen while being evacuated and filled by H_2 (g). This is done to remove any contaminants and oxides from the Cu surface. The pressure at the time of annealing is maintained close to 25 mTorr. Then 35 sccm of CH_4 (g) is introduced along with the 2 sccm of H_2 for 30 min (pressure maintained at ~250 mTorr) after which the furnace was slowly cooled to room temperature. Thicker multilayer graphene (1−8 layers) was grown for the case of Gr/Ni.[12] The high flexibility of graphene makes it conform to the topography of the substrate and strongly adhere to it.[13] However, graphene grown on both Cu and Ni is physisorbed onto these metals, and therefore physical contact with the surface of graphene should be avoided to keep it intact.

Finally, we studied devices where CVD-grown graphene on copper was mechanically transferred onto a surface of a different metal, initially pristine nickel. These samples are particularly interesting, since they represent a strategy we envision for corrosion-protection: graphene is mechanically transferred onto an arbitrary surface that needs to be passivated against corrosion. To vary the thickness of the protective coating, we investigated the samples where two (tr2Gr/Ni) or four (tr4Gr/Ni) graphene layers were transferred successively onto a nickel surface (Figure 1b). The transfer process began with growing a single-layer graphene on copper foils, spin-depositing a layer of PMMA (A7) resist at 4000 rpm for 45 s, making a PMMA/graphene/Cu sandwich, dissolving Cu foil in APS-100 copper etchant. Once the Cu underneath is etched, we fish out the PMMA/graphene stack into DI water baths and carefully deposit it onto the target nickel surface. We let the sample dry at room temperature until the PMMA/graphene is flat on the metal surface then finally dissolve the PMMA with acetone. Once a uniform layer of graphene is deposited onto the nickel, the

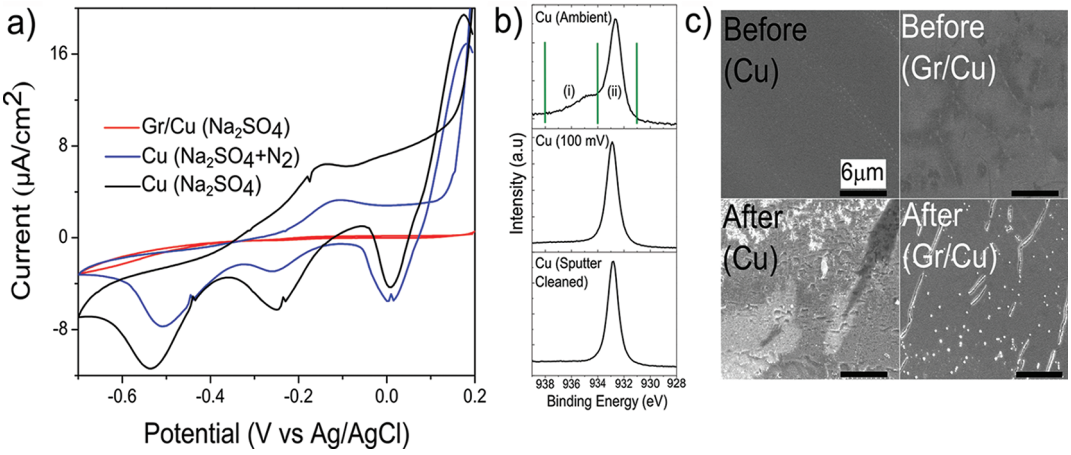

Figure 2. (a) Cyclic voltammetry measurements (electrolyte is 0.1 M Na_2SO_4) in the potential window −700 to 200 mV for bare Cu and Gr/Cu samples. Blue line corresponds to the measurement with nitrogen bubbled through the solution. (b) XPS core level spectrum of Cu (ambient), Cu (100 mV), and Cu (sputter cleaned) samples. The region (i) contains a shoulder due to CuO, the region (ii) contains a peak due to Cu_2O/Metallic Cu. (c) SEM images of Cu and Gr/Cu sample before and after CV scan.

transfer procedure is repeated several times to obtain thicker graphene coatings. The integrity of graphene in all devices was confirmed by Raman spectroscopy.[14]

Cyclic Voltammetry (CV). Our first goal is to elucidate the impact of using graphene as a protective layer on the chemical reactions involved in a corrosion process *via* CV. In the case of bare Cu samples, we expect the corrosion process to comprise anodic oxidation that creates soluble Cu^{2+} ions and cathodic reduction reactions that consume the electrons released from the anodic reaction.[15]

Anodic reaction:

$$Cu \rightarrow Cu^{2+} + 2e^-$$

Cathodic reduction of O_2:[16]

$$O_2 + 2H_2O + 4e^- \rightarrow 4OH^-$$

These two reactions complement each other so that impeding one of them slows the overall corrosion process.

For bare Cu devices, CV measurements provide signatures compatible with these reactions. First, Figure 2a shows that in the positive sweep, bare Cu exhibits a cathodic current that decreases as the potential is made less negative, followed by an anodic peak at −150 mV (*vs*. Ag/AgCl) that we attribute to the formation of adsorbed species on the copper surface. These adsorbed species are then subsequently dissolved as shown by quartz crystal microbalance (QCM) and rotating ring-disk electrode (RRDE) experiments.[17] In the negative sweep, the CV shows additional electrodissolution of copper (200 to −800 mV) that is influenced by the high concentration of H^+ ions near the surface characteristic in Na_2SO_4 media.[18] The CV also shows three cathodic peaks at 0, −250, and −550 mV that we attributed to the electroreduction of copper ions, the reduction of Cu^{2+} to Cu^{1+} species, and the reduction of Cu^{1+} to metallic Cu. To confirm the relation of these peaks to the cathodic reduction of oxygen, we collected the CVs under low oxygen concentration conditions (which was achieved by bubbling N_2 gas through the electrolyte for 10 min) and observed their significant suppression.

In contrast, the Gr/Cu samples do not feature any peaks at negative potentials and exhibit dramatically lower current at positive potentials (red curve in Figure 2a). This provides the first indication that a graphene monolayer exhibits a much lower affinity toward oxygen reduction and forms a barrier between the solution and the copper surface, thereby preventing corrosion.

Three techniques indicate that there is little or no oxide layer formation in the bare copper and graphene-protected copper. First, the CVs do not exhibit anodization maxima associated with the formation of a stable oxide layer.[19] Second, Pourbaix diagrams[16] indicate that upon application of positive potentials to the copper electrode in a $NaSO_4$(aq) electrolyte (pH ∼7), soluble Cu^{2+} ions are produced rather than a stable CuO layer. Finally, the XPS analysis suggests only trace amounts of oxide on the copper surface. Figure 2b shows results from XPS characterization of (i) a Cu sample that has been kept in the ambient atmosphere for over a week, (ii) a Cu sample that has been taken to +100 mV potential in Na_2SO_4, (iii) a sputter-cleaned Cu surface which is free of all oxides. The XPS core-level Cu2p spectrum of sputter-cleaned Cu exhibits a very sharp peak that indicates the lack of copper oxides. In contrast, the copper peak (932 eV) is broadened both in the sample that was kept in the ambient atmosphere and in the samples that were kept at +100 mV in the electrolyte. This broadening is likely caused by the Cu_2O peak (due to the formation of native copper oxide) that is very similar in peak position and fwhm to that of clean Cu metal. However, since the broadening is smaller for

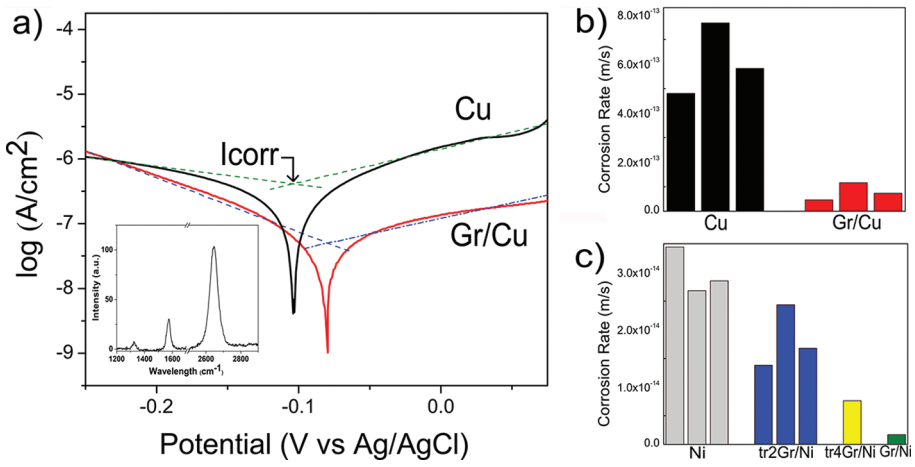

Figure 3. (a) Tafel plots of Cu and Gr/Cu samples. Best fits are represented by dotted lines. Inset: Raman spectrum of the Gr/Cu sample after completing Tafel analysis displays small defect-related "D" peaks. (b) Corrosion rates of Cu and Gr/Cu samples extracted from Tafel plots. (c) Corrosion rates of bare Ni samples and the samples where graphene was transferred onto Ni substrate.

the electrochemically processed sample compared to the sample kept at ambient conditions, we once again conclude that the oxide layer is not formed electrochemically (more information about XPS is in the Supporting Information).

The SEM imaging provides additional information about the nature of corrosion in Gr/Cu devices (Figure 2c). While the entire surface of the bare Cu sample is damaged after exposure to positive potentials (200 mV from the open circuit potential (OCP)) in the electrolytes, in Gr/Cu samples the surface degrades at isolated areas, while leaving most of the sample surface undamaged (Figure 2c). As graphene does not corrode in the potential window used in our experiment, we expect that these changes occur at regions of the copper surface that is not covered by graphene, that is, at cracks in the graphene film.

Interestingly, Raman spectra taken on graphene samples after electrochemical measurements indicate near-pristine and only lightly damaged graphene. For samples taken to positive potentials, we find that graphene is still intact, while a small defect-related D-peak at ~1350 cm^{-1} appears in some of the samples (Figure 3a, inset).[20] This change in the Raman spectra suggests graphene does not exhibit appreciable corrosion at the potentials employed in the experiment.

Tafel Analysis. Having understood the reactions at play, we now turn to quantitative determination of the corrosion rates *via* Tafel analysis. An electrochemical reaction under kinetic control obeys the Butler–Volmer equation, which relates the exponential dependence of current to the deviation of voltage from the open circuit potential value.[21] Therefore, by potentiostatically measuring the dependence and plotting the logarithm of the current density (*I*) *vs.* the electrode potential (*V*) it is possible to extract the reaction kinetic parameters, such as the corrosion rate. All measurements were done using a CH Instruments CHI660a electrochemical workstation with a Faraday cage. We first establish the OCP where the rates of the anodic and cathodic processes are balanced. The OCPs for Cu samples were found to be around −100 mV while for Gr/Cu it was *ca.* −75 mV. The cathodic/anodic branches were obtained by sweeping the voltage −150/150 mV from the OCP using scan rates of 0.005 mV/s. It is notable that the curve for the Gr/Cu sample is shifted to slightly larger potentials and significantly lower currents compared to Cu samples (Figure 3a). We then obtain a linear fit to the data by excluding the part of the curve at large overpotentials (over ±200 mV) and obtain I_{corr} from the point of intersection. The corrosion rate (CR) was calculated using the I_{corr} values:

$$CR = \frac{I_{corr} \times K \times EW}{\rho A}$$

Here, the corrosion rate constant $K = 3272$ mm/year,[22] the equivalent weight EW = 31.7 g for Cu (29 g for Ni), the material density $\rho = 8.94$ g/cm^3 for Cu (8.90 g/cm^3 for Ni), and the sample area $A = 0.4$ cm^2.

For bare metal samples we obtained the rates of $5.76 \times 10^{-13} \pm 1.9 \times 10^{-13}$ m/s for Cu, and $2.99 \times 10^{-14} \pm 4.0 \times 10^{-15}$ m/s for Ni. These values were obtained by averaging over three different samples and are comparable to the literature values.[23] Graphene grown *via* CVD was found to significantly slow down corrosion. For Gr/Cu samples the corrosion rate was $7.85 \times 10^{-14} \pm 3.5 \times 10^{-14}$ m/s, a reduction of ~7 times compared to the bare sample, and for Gr/Ni − 1.71×10^{-15} m/s, a reduction of ~20 times was observed (Figure 3b). Remarkably, graphene, which is only atomically thick, provides the corrosion reduction that is comparable to conventional organic coatings that are more than five times thicker.[24]

We have similarly extracted the corrosion rates for samples where the graphene films grown on copper were mechanically transferred onto a target nickel

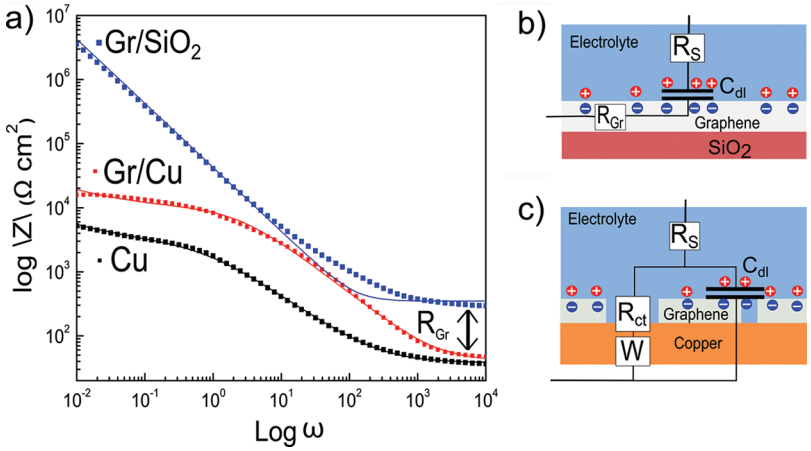

Figure 4. (a) Bode magnitude plots of Gr/SiO_2, Cu, and Gr/Cu samples (solid symbols). Best fits to the equivalent circuit models are solid lines. (b) Equivalent circuit model used in modeling Gr/SiO_2 devices. (c) Equivalent circuit model for Cu and Gr/Cu devices.

substrate. We have found that a single layer of graphene transferred onto nickel does not reduce the corrosion rate of nickel significantly. This is likely a result of tears and rips in the graphene film that may result during its transfer onto the Ni substrate. However, for the case where two or four layers of graphene are transferred onto nickel sequentially, the corrosion rate decreased to 1.83×10^{-14} m/s and to 7.62×10^{-15} m/s, respectively (Figure 3c). The latter value represents a 4-fold reduction of the corrosion rate for bare nickel.

Electrochemical Impedance Spectroscopy. Our final goal is to elucidate the mechanism of corrosion protection by graphene *via* electrochemical impedance spectroscopy (EIS) measurements.[25] In EIS, a small sinusoidal perturbation is applied to the sample under examination and the impedance modulus $|Z|$ is recorded as a function of frequency ω. The analysis of the frequency behavior of the impedance $|Z|$ (ω) allows determination of the corrosion mechanism and the robustness of the coating.[26] Figure 4 shows a Bode magnitude plot ($\log |Z|$ *vs* $\log \omega$) for Gr/SiO_2 (blue squares), Gr/Cu (red), and Cu (black) samples. The observed behaviors can be understood by fitting the data to simple equivalent circuit models.

Qualitatively, the behavior of bare Cu and Gr/SiO_2 samples is consistent with the behavior of an unprotected metal for the former case, and the behavior of a perfectly protected surface for the latter. The Gr/Cu samples exhibit an intermediate behavior consistent with the behavior of a graphene-protected metal with minor defects in the protective coating. At low frequencies, Gr/Cu samples exhibit conductivity similar to that of conductive metal. At intermediate frequencies, the surface favors the collection of charges in a similar way to the way the graphene surface does it, since its capacitive behavior resembles that of Gr/SiO_2. Additionally at high frequencies, the surface exhibits a charge transfer behavior indicative of copper degradation.

The behavior of the typical bare copper sample (Figure 4a, black symbols) adheres to a Randles+Warburg circuit model (shown in Figure 4c) that is typically used for uncoated metals.[27] This network includes the following elements: a resistor $R_S \approx 40 \pm 6.5\ \Omega\ cm^2$ that is due to electrical resistance of the solution, a resistor $R^0_{CT} \approx 2.95 \pm 0.5\ k\Omega\ cm^2$ due to Faradaic charge-transfer resistance between the metal and the liquid (metal corrosion), a Warburg element, $W \approx 1.03 \times 10^{-3}\ \Omega^{-1}s^{(1/2)}/cm^2$ which accounts for linear semi-infinite diffusion,[28] and a constant phase element (CPE) to model the capacitance of the electrical double layer (EDL) at the metal/liquid interface. We translated this CPE information into an equivalent capacitance of $C^0_{DL} \approx 42 \pm 2.2\ \mu F/cm^2$ (CPE terms: $Y_o \approx 7.55 \times 10^{-5}\ \Omega^{-1}\ s^{\alpha}/cm^2$, $\alpha \approx 0.75$).[29] These values were averaged over three measured samples.

To elucidate the contribution to EIS that is due to graphene, before considering Gr/Cu devices, it is instructive to examine Gr/SiO_2 devices, where graphene is transferred onto an insulating substrate. The impedance data for such devices (blue symbols in Figure 4a) adhere to a single capacitance model (blue line). This model includes the solution resistance $R_S \approx 440\ \Omega\ cm^2$, that is now significantly higher compared to the bare Cu samples. We attribute this change in solution resistance to the electrical surface resistance of graphene ($R_{GR} \approx 1000\ \Omega$) in series with a double layer capacitance $C_{DL\_GR} \approx 3.78 \pm 0.06\ \mu F/cm^2$. The adherence of the observed behavior to a capacitive behavior at low frequencies and the absence of charge transfer resistance due to corrosion indicate the absence of graphene corrosion at these conditions.

Finally, the behavior of all measured Gr/Cu devices adheres closely to the same model used for bare Cu (Figure 4a, red symbols). We obtain the average (over three samples) values of $R_S \approx 37.5 \pm 3.0\ \Omega\ cm^2$, $C_{DL} \approx 9.40 \pm 5.0\ \mu F/cm^2$ (CPE parameters: $Y_o \approx 1.85 \times 10^{-5}\ \Omega^{-1}\ s^{\alpha}/cm^2$, $\alpha \approx 0.8$), $W \approx 3.1 \times 10^{-5}\ \Omega^{-1}\ s^{(1/2)}/cm^2$

and $R_{CT} \approx 10.1 \pm 1.2\ k\Omega\ cm^2$. We note that the value of the C_{DL} used in this model (that could be interpreted once again as due to the graphene/liquid EDL capacitance) is ~10 times smaller than C^0_{DL} measured for Cu, which would be surprising if C_{DL} was originating solely from the EDL capacitance. We propose that the difference is a result of the quantum capacitance of graphene—the capacitance contribution that appears in series with the capacitance of the EDL, and is due to the small density of states of graphene. Indeed, the previously reported values for quantum capacitance ($7-10\ \mu F/cm^{-2}$) are close to the observed C_{DL}.[30] The increased value of R_{CT} in comparison with the corresponding R^0_{CT} for Cu samples indicates that only the fraction of the copper that is not covered by graphene is able to participate in the process of corrosion.

We can estimate the fractional area of these uncoated regions *via* $A \approx R^0_{CT}/R_{CT}$[26] Surprisingly, we arrive to a rather large fraction ($A \approx 0.29$), much larger than the estimations from optical microscopy images ($A < 0.05$).[7] We propose that corrosion is initiated at the defects of the graphene film, followed by electrolyte permeation under the graphene surface, leading to a larger apparent corroded area.

CONCLUSION

We have demonstrated that single-layer and multilayer graphene films can serve as corrosion-inhibiting coatings and developed quantitative models that describe the passivation mechanism. We expect that the proposed method of corrosion passivation is quite versatile and is applicable not just to nickel and copper but to arbitrary metallic surfaces that are either smooth or rough.[31] Furthermore, our data indicate that corrosion occurs in the cracks of graphene. The efficiency of the corrosion inhibition may be greatly enhanced by developing protocols to grow highly uniform and large-grain graphene and by performing high fidelity mechanical transfer of graphene onto various metallic surfaces. Finally, we demonstrate that a combination of simple electrochemical techniques can be effectively used to characterize the graphene protective coatings.

METHODS

All electrochemical measurements were performed in a polytetrafluoroethylene (PTFE) three-electrode cell. A platinum wire was used as a counter-electrode, an Ag/AgCl (Gamry Instruments part no. 930-29) was used as a reference electrode, and the sample of interest was used as the working electrode. The Cu and Gr/Cu foils were laterally mounted in the cell exposing a sample area of 0.4 cm^2 (Figure 1a, inset). The sample foils are typically 1 × 1 cm squares. They are clasped onto a 0.4 cm^2 opening on the PTFE cell that houses the electrolyte. An O-ring is used to make a seal between the electrolyte and the outside space. Copper tape is attached to the sample foil to make electrical contact. Once the sample is mounted onto the electrode cell, it is filled with 0.1 M $NaSO_4$ electrolyte. A Pt counter-electrode and Ag/AgCl reference electrode are immersed into the electrolyte.

X-ray photoelectron spectroscopy (XPS) was performed in a Physical Electronics (PHI) VersaProbe 5000 using a monochromatic Al Kα (1486.6 eV) X-ray source. Photoelectrons were collected into a spherical capacitor analyzer operated in constant pass-energy mode from a 200 μm diameter spot irradiated at 50 W. Survey and high-resolution spectra were taken with pass energies of 187.8 and 23.5 eV, respectively. Charge neutralization was achieved with 1.1 eV electrons and 10 Ar^+ ions. Linearity was calibrated to the Ag3d5/2 peak at 368.28 eV. The work function was adjusted so the Au4f7/2 and Cu2p3/2 peaks were separated by 848.6 eV, at 84.05 and 932.65 eV, respectively. Analysis was done using CasaXPS analysis software using the PHI factory provided sensitivity factors.

Conflict of Interest: The authors declare no competing financial interest.

Acknowledgment. This work was supported by NSF EPS 1004083 and NSF CAREER DMR-1056859. We thank AKM Newaz for help with experiments and D. Cliffel for useful discussions.

Supporting Information Available: Elemental surface analysis using XPS to confirm the absence of electrochemical oxide formation on Cu and Gr/Cu samples. This material is available free of charge *via* the Internet at http://pubs.acs.org.

REFERENCES AND NOTES

1. Corrosion Costs and Preventive Strategies in the United States. http://www.nace.org/content.cfm?parentid=1011&currentID=1045 (accessed August 2011).
2. Pushpavanam, M.; Raman., V; Shenoi, B. A. Rhodium—Electrodeposition and Applications. *Surf. Technol.* **1981**, *12*, 351–360.
3. Tallman, D.; Spinks, G.; Dominis, A.; Wallace, G. G. Electroactive Conducting Polymers for Corrosion Control. *J. Solid State Electrochem.* **2002**, *6*, 73–84.
4. Lusk, A. T.; Jennings, G. K. Characterization of Self-Assembled Monolayers Formed from Sodium S-Alkyl Thiosulfates on Copper. *Langmuir* **2001**, *17*, 7830–7836.
5. Sung, M. M.; Kim,Y. Self-Assembled Monolayers of Alkanethiols on Clean Copper Surfaces. *Bull. Korean Chem. Soc.* **2001**, Vol. *22*.
6. Liu, L.; Ryu, S.; Michelle, R; Tomasik, E.; Jung, N.; Hybertsen, M. S.; Steigerwald, M. L.; Brus, L. E.; Flynn, G. W. Graphene Oxidation: Thickness-Dependent Etching and Strong Chemical Doping. *Nano Lett.* **2008**, *8*, 1965–1970.
7. Li, X.; Weiwei, C.; An, J.; Kim, S.; Nah, J.; Yang, D.; Piner, R.; Velamakanni, A.; Jung, I.; Tutuc, E.; *et al.* Large-Area Synthesis of High-Quality and Uniform Graphene Films on Copper Foils. *Science* **2009**, *324*, 1312–1314.
8. Bae, S.; Kim, H.; Lee, Y.; Xu, X.; Park, J. S.; Zheng, Yi.; Balakrishnan, J.; Lei, T.; Kim, H. R.; Song, Y, Il.; *et al.* Roll-to-Roll Production of 30-in. Graphene Films for Transparent Electrodes. *Nat. Nanotechnol.* **2010**, *5*, 574–578.
9. Nair, R. R.; Blake, P.; Grigorenko, A. N.; Novoselov, K. S.; Booth, T. J.; Stauber, T.; Peres, N. M. R.; Geim, A. K. Fine structure Constant Defines Visual Transparency of Graphene. *Science* **2008**, *320*, 5881.
10. Bunch, J. S.; Verbridge, S. S.; Alden, J. S.; van der Zande, A. M.; Parpia, J. M.; Craighead, H. G.; McEuen, P. L. Impermeable Atomic Membranes from Graphene Sheets. *Nano Lett.* **2008**, *8*, 2458–2462.
11. Chen, S.; Brown, L.; Levendorf, M.; Cai, W.; Ju, S. Y.; Edgeworth, J.; Li, X.; Magnuson, C. W.; Velamkanni, A.; Piner,

R. D.; *et al*. Oxidation Resistance of Graphene-Coated Cu and Cu/Ni Alloy. *ACS Nano* **2011**, *5*, 1321–1327.
12. Kim, K. S.; Zhao, Y.; Jang, H.; Lee, S. Y.; Kim, J. M.; Kim, K. S.; Ahn, J.-H.; Kim, P.; Chai, J.-Y.; Hong, B. H. Large-Scale Pattern Growth of Graphene Films for Stretchable Transparent Electrodes. *Nature* **2009**, *457*, 706–710.
13. Koenig, Steven P.; Narashimma., G; Boddeti, Martin.; Bunch, J.Scott. Ultrastrong Adhesion of Graphene Membranes. *Nat. Nanotechnol.* **2011**, *6*, 543–546.
14. Ferrari, A. C.; Meyer, J. C.; Scardaci, V.; Casiraghi, C.; Lazzeri, M.; Mauri, F.; Piscanec, S.; Jiang, D.; Novoselov, K. S.; Roth, S.; Geim, A. K. Raman Spectrum of Graphene and Graphene Layers. *Phys. Rev. Lett.* **2006**, *97*, 187401.
15. Talbot, D; Talbot, J. *Corrosion Science and Technology*, 2nd ed.; CRC Press: New York, 1998.
16. Jones, D. A. *Principles and Prevention of Corrosion*, 2nd ed.; Prentice Hall: NJ, 1995.
17. Jardy, A.; Legal Lasalle-Molin, A.; Keddam, M.; Takenouti, H. Copper Dissolution in Acidic Sulphate Media Studied by QCM and RRDE Under AC Signal. *Electrochim. Acta* **1992**, *37*, 2195–2201.
18. Ismail, K. M.; Fathi, A. M.; Badawy, W. A. Effect of Nickel Content on the Corrosion and Passivation of Copper–Nickel Alloys in Sodium Sulfate Solutions. *Corrosion* **2004**, *60*, 795.
19. Milosev, I.; Metikos-Hukovic, M.; Dragowska, M.; Menard, H.; Brassard, L. Breakdown of Passive Film on Copper in Bicarbonate Solutions Containing Sulfate Ions. *J. Electrochem. Soc.* **1992**, *139*, 2409–2418.
20. Ramesh, P.; Itkis, M. E.; Bekyarova, E.; Wang, F.; Niyogi, S.; Chi, X.; Berger, C.; de Heer, W.; Haddon, R. C. Electro-oxidized Epitaxial Graphene Channel Field-Effect Transistors with Single-Walled Carbon Nanotube Thin Film Gate Electrode. *J. Am. Chem. Soc.* **2010**, *132*, 14429–14436.
21. Bard, A. J.; Faulkner, L. R. *Electrochemical Methods: Fundamentals and Applications*, 2nd ed.; Wiley: New York, 2000.
22. Gamry Instruments: Getting Started with Electrochemical Corrosion Measurement. http://www.gamry.com/assets/Application-Notes/Getting-Started-with-Electrochemical-Corrosion-Measurement.pdf (accessed August 2011).
23. Kreysa, G; Schutze, M. *Dechema Corrosion Handbook: Sodium Dioxide, Sodium Sulfate*, 2nd ed.; Dechema: Frankfurt, Germany, 2008.
24. Laibinis, P. E.; Bain, C. D.; Nuzzo, R. G.; Whitesides, G. M. Structure and Wetting Properties of ω-Alkoxy-*n*-alkanethiolate Monolayers on Gold and Silver. *J. Phys. Chem.* **1995**, *99*, 7663–7676.
25. Mansfeld, F. Electrochemical Impedance Spectroscopy (EIS) as a New Tool for Investigating Methods of Corrosion Protection. *Electrochim. Acta* **1990**, *35*, 1533–1544.
26. Amirudin, A.; Thieny, D. Application of Electrochemical Impedance Spectroscopy To Study the Degradation of Polymer-Coated Metals. *Prog. Org. Coat.* **1995**, *26*, 1–28.
27. Jennings, G. K.; Munro, J. C.; Yong, T.-H.; Laibinis, P. E. Effect of Chain Length on the Protection of Copper by *n*-Alkanethiols. *Langmuir* **1998**, *14*, 6130–6139.
28. Gamry Instruments Application Notes. http://www.gamry.com/App_Notes/EIS_Primer/Basics_Of_%20EIS.pdf (accessed August 2011).
29. Hirschorn, Bryan.; Orazem, M. E.; Tribollet, B.; Viver, V.; Frateur, I.; Musiani, M. Determination of Effective Capacitance and Film Thickness from Constant-Phase-Element Parameters. *Electrochim. Acta* **2010**, *55*, 6218–6227.
30. Xia, J; Chen, F; Li, J.; Tao, N. Measurement of the Quantum Capacitance of Graphene. *Nat. Nanotechnol.* **2009**, *4*, 505–509.
31. Sutter, E.; Albrecht, P; Camino, F. E.; Sutter, P. Monolayer Graphene as Ultimate Chemical Passivation Layer for Arbitrarily Shaped Metal Surfaces. *Carbon* **2010**, *48*, 4414–4420.